Geometry and vibrations of N-methylpyrrole in the So state studied by dispersed fluorescence spectroscopy and ab initio calculations

ARTICLE *in* CHEMICAL PHYSICS · AUGUST 2003

Impact Factor: 1.65 · DOI: 10.1016/S0301-0104(03)00299-4

3 AUTHORS:

Nandita Maiti
Department of Atomic Energy
34 PUBLICATIONS **284** CITATIONS
SEE PROFILE

Sanjay Wategaonkar
Tata Institute of Fundamental Research
72 PUBLICATIONS **949** CITATIONS
SEE PROFILE

John Philis
University of Ioannina
53 PUBLICATIONS **688** CITATIONS
SEE PROFILE

Available online at www.sciencedirect.com
SCIENCE DIRECT®
Chemical Physics 293 (2003) 99–109
Chemical Physics
www.elsevier.com/locate/chemphys

Geometry and vibrations of *N*-methylpyrrole in the S_0 state studied by dispersed fluorescence spectroscopy and ab initio calculations

N. Biswas[a], S. Wategaonkar[a], John G. Philis[b,*]

[a] *Department of Chemical Sciences, Tata Institute of Fundamental Research, Colaba, Mumbai 400005, India*
[b] *Department of Physics, University of Ioannina, GR-45110 Ioannina, Greece*

Received 24 February 2003

Abstract

A number of vibrational frequencies in the ground state of *N*-methylpyrrole ($C_4H_4NCH_3$) have been determined via laser-induced dispersed fluorescence spectra recorded under jet-cooled conditions. Eight vibronic levels of the symmetry forbidden $3s(A_2)S_1 \leftarrow (A_1)S_0$ Rydberg transition were pumped including the methyl rotor levels 2e′, 3+, 3− and 4e′. The DF spectra provided a detailed look of the S_1–S_0 inducing modes. The geometrical structure and the vibrational modes of NMP in the S_0 electronic state have been calculated at the DFT and MP2 level using two basis sets, 6-311G** and D95++. The barrier for the methyl group rotation is also calculated.

1. Introduction

Recent one-photon REMPI experiments [1,2] on jet-cooled *N*-methylpyrrole, (NMP), demonstrated the activity of the methyl internal rotation in the $S_1 \leftarrow S_0$ electronic transition. This transition is not of ππ* valence type, but it is the electric dipole forbidden $(3s)A_2 \leftarrow A_1$ Rydberg transition. Theoretical results on pyrrole show that this transition is of πσ* type exhibiting pronounced charge-transfer character [3]. It is the lowest lying transition ($E_{3s} = 5.107$ eV, 243 nm region) in the absorption spectrum of NMP because of the relatively low ionization energy (*IE*) of NMP ($IE = 7.95$ eV). From the Rydberg formula

$$E_{3s} = IE - R/(3-\delta)^2 \quad (1)$$

the quantum defect value $\delta = 0.82$ is derived (the constant $R = 13.605$ eV). The $(A_2)S_1 \leftarrow S_0$ transition is weak in the absorption spectrum [4,5] and its origin has been detected in two-photon REMPI experiments [1,2,5,6].

The forbidden character of the $S_1 \leftarrow S_0$ transition and the appearance of methyl rotor transitions establish NMP as an interesting molecule for further spectroscopic studies. Laser-induced fluorescence excitation (FE) and dispersed fluorescence (DF) spectra of NMP have not been reported in the literature. Such experiments,

* Corresponding author. Tel.: +30-2651098530; fax: +30-2651098695.
E-mail addresses: sanwat@tifr.res.in (S. Wategaonkar), iphilis@cc.uoi.gr (J.G. Philis).

0301-0104/$ - see front matter © 2003 Elsevier Science B.V. All rights reserved.
doi:10.1016/S0301-0104(03)00299-4

especially when performed under jet-cooled conditions, provide valuable information about the electronic and vibrational structure of the molecule. By pumping single vibronic levels, the DF spectra can provide the active vibrations in the ground state, constrained by the symmetry selection rules and the Franck–Condon factors.

The present work is focused on the geometrical and vibrational properties of the *N*-methylpyrrole ground state. Eight DF spectra have been obtained after exciting various transitions observed in the one photon excitation spectrum of the jet-cooled NMP. For molecules, which fall into the low barrier category, the usual practice has been to classify the normal vibrations according to the irreducible representation of the "frame" group. Defining the pyrrole ring as the frame, the proper symmetry to discuss the $S_1 \leftarrow S_0$ transition is the C_{2v} point group.

IR and Raman data for NMP are scattered in the literature and have been collected by Scott [7] in a theoretical work on the valence force fields of furan, pyrrole and their methyl derivatives. Very recently, Dines et al. [8] studied the IR spectroscopy of NMP adsorbed on oxides and presented their experimental data for the vibrational modes above 1000 cm^{-1}. The calculated vibrational fundamentals (B3-LYP/DZ++ level) were also included in their work [8]. Huber et al. [9] reported the optimized structure calculated at the MP2 level with 6-311G** basis set whose geometrical parameters are in good agreement with the recently refined experimental structural data [10]. However, they did not report the normal mode frequencies. In this work we report the optimized structural parameters and normal mode frequencies for the ground state calculated using various basis sets. The methyl torsional barrier was also calculated using ab-initio methods. The normal mode frequencies are compared with the vibrational modes observed in the laser-induced dispersed fluorescence (DF) spectra.

2. Experimental

The fluorescence excitation and dispersed fluorescence spectra were recorded under jet-cooled conditions in order to characterize its excited (S_1) and ground (S_0) electronic states. Briefly, the experiments were carried out using a 500 μm diameter pulsed nozzle driven by a pulsed valve driver (General Valve Corporation; IOTA ONE). A 10 Hz nanosecond Nd^{3+}:YAG laser (Quantel YG781C) pumped dye laser (Quantel TDL70) was used to provide the tunable excitation source for the excitation spectra and the dispersed fluorescence spectra. The wavelength range of interest (240–246 nm) was generated by mixing the frequency doubled output of the DCM+SR640 (Exciton Inc.) dye (620–640 nm) with the 1064 nm fundamental of the YAG laser. The line width of the dye laser output was ~ 0.3 cm^{-1} and the typical pulse energies were ~ 200 μJ. The total fluorescence was detected by a PMT/Filter combination (1P28, BG3) for recording the excitation spectra. The dispersed fluorescence was monitored using a monochromator (McPherson, 2035, 0.35 m) and PMT (Hamamatsu R943). The typical resolution in the dispersed fluorescence spectra was 10–15 cm^{-1}. The signal was digitized and averaged using a digital storage oscilloscope (Lecroy 9450A).

N-Methylpyrrole (NMP), a liquid at room temperature, has sufficient vapor pressure to record excitation and dispersed fluorescence spectra with a good S/N ratio. It was purchased from Aldrich Chemicals Company (99%) and used without further purification. The buffer gas, a 20% mixture of argon in helium was from the local commercial sources and was used without further purification. The typical stagnation pressure was 2 atm and the working pressure in the fluorescence chamber was $\sim 10^{-4}$ Torr.

3. Normal modes of vibrations

The normal vibrations of NMP need to be numbered, because this numbering has not been given in the literature. The 33 vibrations of NMP are the sum of 24 ring modes, 8 vibrations of the methyl group and 1 methyl torsion (twisting). The eclipsed conformation of NMP belongs to the C_s point group (the pyrrole ring is the σ_h plane) while the staggered conformation is again C_s but the σ_h plane is perpendicular to the pyrrole ring. Taking

Table 1
Numbering of the normal modes of vibrations in *N*-methylpyrrole (C_{2v} symmetry). The calculated frequencies (in cm^{-1}) are unscaled. IR and Raman data are from [7,8]

Symmetry	Mode	Description	B3LYP/6 311G**	IR and Raman
a_1	ν_1	C–H stretch (ring)	3256.3	3126
	ν_2	C–H stretch (ring)	3235.9	3101
	ν_3	methyl C–H_3 sym str	3023.6	2812
	ν_4	CH_3 umb + ring def + N–C str + C–H ip bend	1539.3	1509
	ν_5	CH_3 umbrella mode	1453.5	1447
	ν_6	ring def + C–H ip bend	1420.1	1419
	ν_7	ring breathing + N-CH_3 str	1320.3	1288
	ν_8	C–H ip bend + C–C ring def	1108.8	1091
	ν_9	C–H ip bend + C–C ring def	1078.1	1055
	ν_{10}	N–C(r) sym str + C–H ip bend	985.5	966
	ν_{11}	ip ring def + N-CH_3 str	673.4	662
a_2	ν_{12}	C–H op bending	871.3	858
	ν_{13}	C–H op bending	681.0	688
	ν_{14}	op ring deformation	628.1	
	ν_{15}	–CH_3 torsion	84.1	
b_1	ν_{16}	met C–H_3 asym str	3090.3	2907
	ν_{17}	met CH_2 bend	1491.7	
	ν_{18}	CH_3 op rock	1143.2	
	ν_{19}	C–H op bending	817.7	815
	ν_{20}	C–H op bending	724.7	720
	ν_{21}	N Inversion + C–H op bend	618.2	601
	ν_{22}	N–C(methyl) op bend	189.5	186
b_2	ν_{23}	C–H stretch (ring)	3248.3	3130
	ν_{24}	C–H stretch (ring)	3225.6	3103
	ν_{25}	met C–H_3 asym str	3120.8	2943
	ν_{26}	C–C ring def	1555.5	1544
	ν_{27}	met CH_2 bend	1515.2	
	ν_{28}	N–C(r) asym str + CH_3 ip rock	1398.7	
	ν_{29}	C–H ip bend	1294.8	1232
	ν_{30}	C–H ip bend + CH_3 ip rock	1105.9	
	ν_{31}	C–H ip bend + CH_3 ip rock	1061.3	1043
	ν_{32}	ip ring def	890.2	868
	ν_{33}	N-CH_3 ip bend	358.8	354

into consideration that the methyl rotor barrier is low [1], we have chosen to number the vibrations in the approximation of C_{2v} symmetry. The normal modes are grouped together by symmetry species, in the order a_1, a_2, b_1, b_2, and numbered in the decreasing order of energy (Mulliken convention [11]). The B3LYP/6-311G** calculated values (see Section 5.1) have been used to classify the normal modes and this numbering is given in Table 1. IR and Raman data [7,8] are included in this Table.

4. Experimental results – analysis

4.1. Laser-induced fluorescence excitation spectrum

The $(3s)A_2 \leftarrow A_1$ laser-induced fluorescence excitation spectrum (FE) of jet-cooled NMP is displayed in Fig. 1. The (1 + 1) REMPI spectrum [2] is included in this figure. These two spectra are similar and the comparison shows that (a) the methyl internal rotational transitions m_x^y [1,2] are present in the FE spectrum too and (b) the fluo-

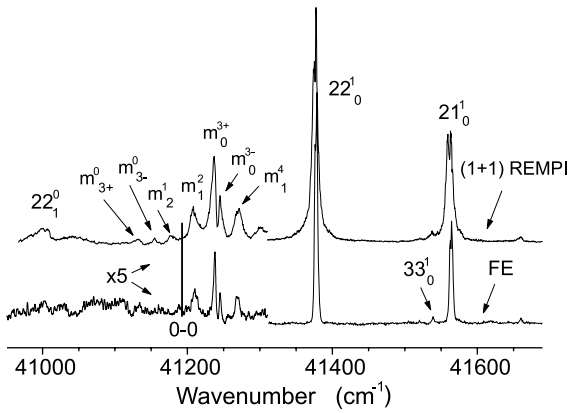

Fig. 1. Part of the 3s $A_2 \leftarrow A_1$ fluorescence excitation (FE) and (1 + 1) REMPI spectrum of jet-cooled NMP. The vertical line at 41,193 cm^{-1} marks the forbidden origin of this transition.

rescence quantum yield is constant over the common scanned wavelength region. The peaks of the FE spectrum are sharper than those in the REMPI spectrum because of the low jet-beam temperature achieved in the FE apparatus. The vibronic assignment of the peaks in Fig. 1 is supported by the DF spectra. The missing $S_1 \leftarrow S_0$ origin is at 41,193 cm^{-1}.

The present work shows that the first strong peak at 41,376 cm^{-1} = 41,193 + 183 cm^{-1} (Fig. 1) is not the m_0^{6-} transition as reported previously [1], but it is the b_1 N-CH_3 out of plane bend, 22^1_0. The mechanism for the observed vibronic activity in the symmetry forbidden $(A_2)S_1 \leftarrow (A_1)S_0$ transition is the vibronic coupling between the S_1 state and the B_2 valence state which lies at 5.4 eV i.e., very close to S_1 (see Fig. 1 of [5]). The coupling between a vibronic level in S_1 and an S_n state can appear when both have the same symmetry. The respective irreducible representations of the states that are involved must satisfy the equation

$$\Gamma(S_1) \otimes \Gamma(H_{VC}) = \Gamma(S_n), \tag{2}$$

where H_{VC} represents the vibronic coupling operator that corresponds to the specific active vibration in S_1. Therefore, for an out-of-plane b_1 mode to be active the $\Gamma(S_n)$ must be B_2, for an in-plane b_2 mode to be active the $\Gamma(S_n)$ must be B_1, and for an a_2 mode to be active the $\Gamma(S_n)$ must be A_1. In addition, transitions that involve a combination of two vibrations of different symmetry are permissible, but transitions that involve only two quanta of the same vibrational species are forbidden. Furthermore, a favorable Franck–Condon overlap is necessary for the vibrational modes to contribute to the spectral intensity.

The peak 21^1_0 at 41,563 = 41,193 + 370 cm^{-1} is due to another b_1 vibration, the {N inversion + CH op bend} normal mode. The weak peak at 41,537 = 41,193 + 344 cm^{-1} is assigned as 33^1_0 {N-CH_3 in plane bend} which is b_2. The mechanism for the appearance of this weak peak must be

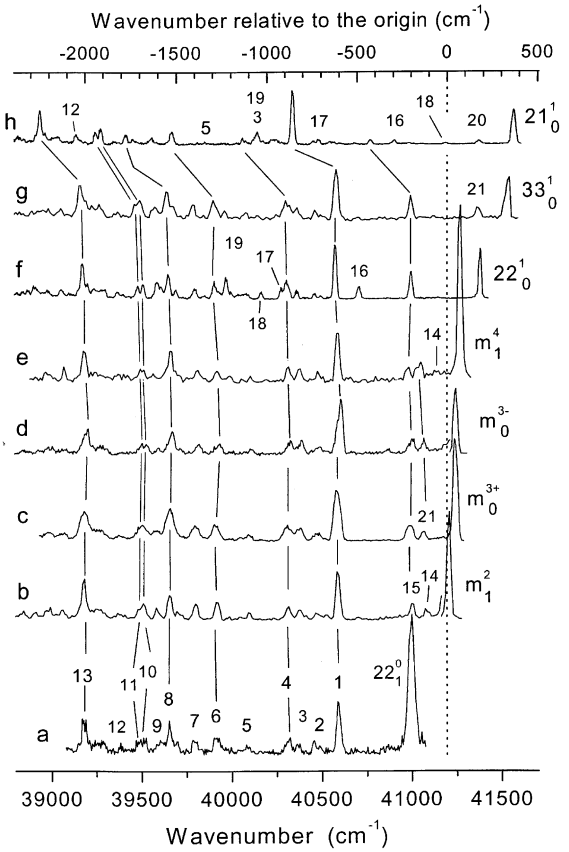

Fig. 2. Dispersed fluorescence spectra of jet-cooled NMP obtained by pumping certain S_1 levels. For spectrum a, the vibrationless S_1 state was pumped via the 22^0_1 hot band. For the other spectra, b–h, the pumped level is indicated on the right. The peaks have been numbered 1 to 21 and the peaks with same numbers are connected with lines. For the clarity of the figure, the eye-guide lines for the peaks numbered as 2, 3, 5, 7, 9, 12 are not drawn. The resonance lines m_1^2 and m_0^{3-} have been reduced by a factor of 10.

the coupling to a B_1 state and we propose that this state is the $3p_y$ Rydberg ($\delta = 0.53$), present at 5.713 eV (217 nm) in the absorption spectrum [5].

4.2. Dispersed fluorescence spectra

Eight dispersed fluorescence spectra, [a]–[h], have been obtained by pumping the following S_1 levels. The excitation energies are given in parenthesis: [a] vibrationless S_1 (40,999 cm^{-1}), via 22_1^0, [b] m^2 (41,208 cm^{-1}), [c] m^{3+} (41,237 cm^{-1}), [d] m^{3-} (41,244 cm^{-1}), [e] m^4 (41,269 cm^{-1}), [f] 22^1 (41,376 cm^{-1}), [g] 33^1 (41,537 cm^{-1}), [h] 21^1 (41,563 cm^{-1}). These DF spectra are depicted in Fig. 2. All these spectra have been normalized on the intensity of peak #1. The peaks have been arbitrarily numbered in order to facilitate the discussion and the tabulated presentation.

For the interpretation of the DF spectra, the forbidden character of the $(A_2)S_1 \leftarrow (A_1)S_0$ transition has to be taken into consideration. By using the symbol P^1 for the pumped level, the symbol V for a b_1 or b_2 vibration (inducing modes) and the symbol A for a totally symmetric vibration, the peaks can be assigned as $P_1^1V_1^0$, $P_1^1V_1^0A_1^0$, $P_0^1A_1^0$. When a methyl rotor level is involved, the symbol m has to be used instead of the symbol P. For the assignments we were guided by the theoretically calculated frequencies of the normal modes (Table 1). It can be seen from Fig. 2 that the {N inversion + CH op bend} b_1 mode, ν_{21}, is the most active in all the DF spectra (peak #1). This strong transition is assigned as $m_n^n 21_1^0$ in the b–e spectra of Fig. 2 and we call it the pseudo-origin (PO) band. To the left of the PO band, the DF spectra are identical in all the cases, a–h. The complexity of

Table 2
Analysis-assignment of the transitions observed in the DF spectra a–h of Fig. 2

Peak #	DF a	DF b	DF c	DF d	DF e	DF f	DF g	DF h
1	21_1^0	$m_2^2\ 21_1^0$	$m_{3+}^{3+}\ 21_1^0$	$m_{3-}^{3-}\ 21_1^0$	$m_4^4\ 21_1^0$	$22_1^1 21_1^0$	$33_1^1 21_1^0$	21_2^1
2	20_1^0	$m_2^2\ 20_1^0$	$m_{3+}^{3+}\ 20_1^0$	$m_{3-}^{3-}\ 20_1^0$	$m_4^4\ 20_1^0$	$22_1^1 20_1^0$ & $22_0^1 10_1^0$	$33_1^1 20_1^0$	$21_1^1 20_1^0$
3	19_1^0	$m_2^2\ 19_1^0$	$m_{3+}^{3+}\ 19_1^0$	$m_{3-}^{3-}\ 19_1^0$	$m_4^4\ 19_1^0$	$22_1^1 19_1^0$	$33_1^1 19_1^0$	$21_1^1 19_1^0$ & $21_0^1 6_1^0$
4	32_1^0	$m_2^2\ 32_1^0$	$m_{3+}^{3+}\ 32_1^0$	$m_{3-}^{3-}\ 32_1^0$	$m_4^4\ 32_1^0$	$22_1^1 32_1^0$	$33_1^1 32_1^0$	$21_1^1 32_1^0$
5	18_1^0	$m_2^2\ 18_1^0$	$m_{3+}^{3+}\ 18_1^0$	$m_{3-}^{3-}\ 18_1^0$	$m_4^4\ 18_1^0$		$33_1^1 18_1^0$	$21_1^1 18_1^0$
6	$21_1^0 11_1^0$	$m_2^2\ 21_1^0 11_1^0$	$m_{3+}^{3+}\ 21_1^0 11_1^0$	$m_{3-}^{3-}\ 21_1^0 11_1^0$	$m_4^4\ 21_1^0 11_1^0$	$22_1^1 21_1^0 11_1^0$	$33_1^1 21_1^0 11_1^0$	$21_2^1 11_1^0$
7	$20_1^0 11_1^0$	$m_2^2\ 20_1^0 11_1^0$	$m_{3+}^{3+}\ 20_1^0 11_1^0$	$m_{3-}^{3-}\ 20_1^0 11_1^0$	$m_4^4\ 20_1^0 11_1^0$	$22_1^1 20_1^0 11_1^0$	$33_1^1 20_1^0 11_1^0$	$21_1^1 20_1^0 11_1^0$
8	$21_1^0 10_1^0$	$m_2^2\ 21_1^0 10_1^0$	$m_{3+}^{3+}\ 21_1^0 10_1^0$	$m_{3-}^{3-} 21_1^0 10_1^0$	$m_4^4\ 21_1^0 10_1^0$	$22_1^1 21_1^0 10_1^0$	$33_1^1 21_1^0 10_1^0$	$21_2^1 10_1^0$
9	$22_1^0 6_1^0$	$m_2^2\ 22_1^0 6_1^0$	$m_{3+}^{3+}\ 22_1^0 6_1^0$	$m_{3-}^{3-}\ 22_1^0 6_1^0$	$m_4^4\ 22_1^0 6_1^0$	$22_2^1 6_1^0$	$33_1^1 22_1^0 6_1^0$	$21_1^1 22_1^0 6_1^0$
10*	$21_1^0 9_1^0$	$m_2^2\ 21_1^0 9_1^0$	$m_{3+}^{3+}\ 21_1^0 9_1^0$	$m_{3-}^{3-}\ 21_1^0 9_1^0$	$m_4^4\ 21_1^0 9_1^0$	$22_1^1 21_1^0 9_1^0$	$33_1^1 21_1^0 9_1^0$	$21_2^1 9_1^0$
11*	$21_1^0 8_1^0$	$m_2^2\ 21_1^0 8_1^0$	$m_{3+}^{3+}\ 21_1^0 8_1^0$	$m_{3-}^{3-}\ 21_1^0 8_1^0$	$m_4^4\ 21_1^0 8_1^0$	$22_1^1 21_1^0 8_1^0$	$33_1^1 21_1^0 8_1^0$	$21_2^1 8_1^0$
12	$32_1^0 10_1^0$	$m_2^2\ 32_1^0 10_1^0$	$m_{3+}^{3+}\ 32_1^0 10_1^0$		$m_4^4\ 32_1^0 10_1^0$	$22_1^1 32_1^0 10_1^0$	$33_1^1 32_1^0 10_1^0$	$21_1^1 32_1^0 10_1^0$
13	$21_1^0 6_1^0$	$m_2^2\ 21_1^0 6_1^0$	$m_{3+}^{3+}\ 21_1^0 6_1^0$	$m_{3-}^{3-}\ 21_1^0 6_1^0$	$m_4^4\ 21_1^0 6_1^0$	$22_1^1 21_1^0 6_1^0$	$33_1^1 21_1^0 6_1^0$	$21_2^1 6_1^0$
14		m_5^2			m_5^4			
15	22_1^0	$m_2^2\ 22_1^0$	$m_{3+}^{3+}\ 22_1^0$	$m_{3-}^{3-}\ 22_1^0$	$m_4^4\ 22_1^0$	22_2^1	$33_1^1 22_1^0$	$21_1^1 22_1^0$
16						$22_0^1 11_1^0$		$21_0^1 11_1^0$
17						$22_0^1 9_1^0$		$21_0^1 9_1^0$
18						$22_0^1 21_2^0$		$21_0^1 22_2^0$
19						$22_0^1 6_1^0$		$21_0^1 6_1^0$ & $21_1^1 19_1^0$
20								$21_0^1 m_{6+}^0$
21**			171 cm^{-1}	178 cm^{-1}	222 cm^{-1}		180 cm^{-1}	

The first column refers to the numbering of the peaks as given in Fig. 2. Vibrations ν_6, ν_8, ν_9, ν_{10}, ν_{11}, are a_1. Vibrations ν_{18}, ν_{19}, ν_{20}, ν_{21}, ν_{22}, are out-of-plane b_1. Vibrations ν_{32}, ν_{33}, are in-plane b_2.

* Peaks #10 and #11 are well resolved in the DF spectra f and h.

** Peaks #21 are unassigned. The separation (cm^{-1}) of each peak from the respective resonance transition is given in this row.

this region is clarified after the identification of the Franck–Condon (FC) active transitions to totally symmetric vibrations. We have identified five a_1 vibrations, ν_6, ν_8, ν_9, ν_{10}, and ν_{11} combined with the PO band (peak numbers 13, 11, 10, 8, and 6, respectively in Fig. 2). The analysis of the DF spectra yields the value 607 cm^{-1} to mode ν_{21} (S_0 state). This vibration is reduced to 370 cm^{-1} in the S_1 state. This reduction parallels the case of planar aromatic molecules, where some normal modes, particularly the out-of-plane, suffer great reduction in the excited state. The classical example is benzene and its well-known e_{2u} ($\nu''_{16} = 399$ cm^{-1}, $\nu'_{16} = 237$ cm^{-1}) and e_{1g} ($\nu''_{10} = 846$ cm^{-1}, $\nu'_{10} = 581$ cm^{-1}) modes which are active as overtones [12,13]. The complete assignments/interpretation of the transitions in the DF spectra are given in Table 2 and the S_0 vibrational fundamentals that were extracted are listed in Table 3, in the column "Disp. Fluor.". The theoretical frequencies (unscaled) are also included in Table 3. Vibrations ν_{21} and ν_{22} are not the only active (inducing) vibrations in the DF spectra. For the interpretation of the peaks #2 and #3, two other vibrations of b_1

Table 3
Calculated frequencies of *N*-methylpyrrole (unscaled, S_0 state, C_{2v} symmetry)

Symmetry	Mode	B3LYP/D95++	MP2/D95++	B3LYP/6 311G**	MP2/6-311G**	Disp. fluor.
a_1	ν_1	3297.2	3274.1	3256.3	3296.9	
	ν_2	3269.7	3246.6	3235.9	3276.0	
	ν_3	3036.0	3033.5	3023.6	3080.7	
	ν_4	1540.9	1531.1	1539.3	1561.0	
	ν_5	1470.0	1468.8	1453.5	1468.1	
	ν_6	1425.2	1398.7	1420.1	1441.1	1398
	ν_7	1314.3	1285.3	1320.3	1333.6	
	ν_8	1121.4	1120.6	1108.8	1113.4	1083
	ν_9	1083.0	1073.8	1078.1	1100.8	1058
	ν_{10}	981.1	969.0	985.5	985.7	925
	ν_{11}	669.1	654.6	673.4	676.7	669
a_2	ν_{12}	917.3	647.6	871.3	793.2	
	ν_{13}	738.9	488.6	681.0	633.7	
	ν_{14}	628.2	394.4	628.1	580.7	
	ν_{15}	54.4	92.2	84.1	104.0	
b_1	ν_{16}	3115.0	3124.4	3090.3	3161.1	
	ν_{17}	1517.6	1520.5	1491.7	1509.0	
	ν_{18}	1154.7	1166.4	1143.2	1160.3	1100
	ν_{19}	868.7	631.1	817.7	763.0	820
	ν_{20}	752.9	597.7	724.7	704.8	718
	ν_{21}	623.0	544.8	618.2	605.3	607
	ν_{22}	209.7	163.1	189.5	185.7	190
b_2	ν_{23}	3283.2	3258.9	3248.3	3287.3	
	ν_{24}	3259.3	3237.8	3225.6	3266.7	
	ν_{25}	3147.5	3151.0	3120.8	3193.2	
	ν_{26}	1546.6	1495.9	1555.5	1545.2	
	ν_{27}	1529.7	1552.1	1515.2	1541.8	
	ν_{28}	1393.8	1394.5	1398.7	1454.1	1388
	ν_{29}	1310.9	1306.3	1294.8	1290.2	
	ν_{30}	1119.8	1124.9	1105.9	1115.6	
	ν_{31}	1062.8	1060.1	1061.3	1068.6	
	ν_{32}	893.4	887.9	890.2	880.4	877
	ν_{33}	356.8	347.9	358.8	355.1	354

The experimental values are in the last column. All vibrational frequencies are in cm^{-1}.

symmetry, ν_{20} and ν_{19}, respectively, must be involved as inducing modes. Peak #4 is induced by a b_2 vibration, ν_{32}. For peak #5 two explanations exist: the ν_{18} b_1 {CH_3 out-of-plane rock} and the ν_{30} b_2 {CH in-plane bend + CH_3 in-plane rock} normal mode. The former case is tentatively accepted and included in Tables 2 and 3.

In spectrum h of Fig. 2, the separation of peak #1, (21_2^1), from the resonance 21_0^1, is 1228 cm^{-1} which means that the second quanta of ν_{21}'' is 621 cm^{-1}. This also indicates the anharmonic nature of the inversion potential in this molecule. The position of peak #20 in the DF spectrum h is −193 cm^{-1} from the resonance line and we assigned it as the m_{6+}^0 level of the methyl rotor. This value is in agreement with the theoretical value of 195.7 cm^{-1} (totally symmetric 6+ methyl rotor level), calculated with $V_6 = -45$ cm^{-1} [1].

Each DF spectrum, generated by pumping an S_1 methyl rotor level (Fig. 2, spectra b–e), gives the $m_n^n 21_1^0$ transition, labeled as peak #1. From the energy position of each peak #1 and using $\nu_{21}'' = 607$ cm^{-1}, we find the methyl rotor levels in the 21_1 S_0 state: $2e' = 21$ cm^{-1}, $3+ = 53$ cm^{-1}, $3- = 34$ cm^{-1} and $4e' = 77$ cm^{-1} (all are relative to the $0a_1' = 0$ cm^{-1} level). The comparison of these values with the values $2e' = 20.5$ cm^{-1}, $3+ = 60.5$ cm^{-1}, $3- = 38.1$ cm^{-1} and $4e' = 88.8$ cm^{-1} shows that the internal rotational constant F and the methyl potential barrier are mode sensitive. The last set of rotor values is for the vibrationless S_0

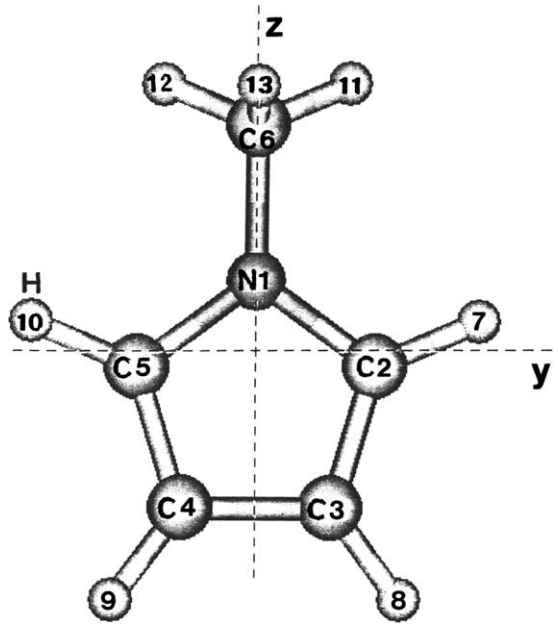

Fig. 3. Optimized structure of *N*-methylpyrrole with atom numbering.

Table 4
Structural parameters of *N*-methylpyrrole calculated using various basis sets at the B3LYP and MP2 level. The bond distances are in Å and the angles in degrees

Parameter	B3LYP/D95++	MP2/D95++	B3LYP/6-311G**	MP2/6-311G**	Expt. data[a]
r(N–C2)	1.392	1.406	1.376	1.372	1.372
r(C2–C3)	1.393	1.413	1.377	1.389	1.383
r(C3–C4)	1.436	1.450	1.421	1.420	1.425
r(N–C6)	1.465	1.483	1.451	1.452	1.452
r(C2–H7)	1.082	1.088	1.078	1.082	1.079
r(C3–H8)	1.082	1.088	1.079	1.081	1.081
r(C6–H13)	1.099	1.103	1.095	1.094	1.1
∠C6–N–C2	125.5	125.2	125.4	125.1	
∠C5–N–C2	108.8	109.3	108.9	109.5	109.3
∠N–C2–C3	108.3	108.0	108.3	108.1	108.2
∠C2–C3–C4	107.3	107.4	107.3	107.2	107.1
∠N–C2–H7	121.1	121.1	120.7	120.7	117.7
C2–C3–H8	125.8	125.6	125.8	125.7	124.0
∠N–C6–H11	109.8	109.0	109.6	109.2	109.9
∠H11–C6–H12	108.3	108.9	108.3	108.7	109.1
d∠(C_5–N–C_6–H_{13})	87.7	86.4	86.9	86.4	

[a] Ref. [10].

state [1]. The spectra c and d of Fig. 2 show clearly that the conformation of the methyl group with respect to the ring plane is not the same in the S_0 and S_1 states. The ordering of the $m = \pm 3$ methyl rotor levels is $3- > 3+$ if the conformation is eclipsed and $3+ > 3-$ if the conformation is staggered. The former case is true for the S_1 state ($3- = 51\ cm^{-1}$, $3+ = 44\ cm^{-1}$) and the latter case is true for the S_0 state.

5. Theoretical computations

Ab-initio calculations were carried using the Gaussian 98 suite of programs [14] at the DFT (using a hybrid functional, B3LYP) and MP2 level using two basis sets viz. 6-311G** and the Dunning/Huzinaga full double zeta basis set with diffused functions, D95++. Fig. 3 shows the optimized structure of NMP with the atom numbering. The optimized geometrical parameters at various levels and basis sets are given in Table 4 along with the experimental data from [10]. These experimental data are the result obtained [10] by a joint analysis of gas electron diffraction and rotational constants [9]. At a glance it can be noticed that the structural parameters calculated at the MP2 level with the 6-311G** basis set agree the best with the experimentally determined structure and also with those reported by Huber et al. [9]. Although both the basis sets give similar C–H bond distances, the C–C and N–C bond distances given by the double zeta basis set are consistently longer at both the levels of calculations. As far as the bond angles are concerned both the basis sets show similar trend, i.e., the bond angles within the ring are better computed compared to those made by the ring hydrogens. The latter are overestimated at both the levels. The angles made by the methyl hydrogens are better predicted however, by both the basis sets. The equilibrium structure for the ground state shows that one of the methyl C–H bonds is perpendicular to the ring plane (staggered conformation). The staggered conformation is the experimentally accepted conformation deduced from the rotational spectra of NMP and NMP–argon complexes [15].

5.1. Vibrational modes of the electronic ground state

Table 3 lists all the computed normal modes (unscaled frequencies). The dispersed fluorescence results are included in Table 3. Although both the basis sets fairly adequately reproduce the experimentally observed frequencies at the B3LYP level, at the MP2 level some of the calculated frequencies are smaller than the observed ones contrary to the general observation that the computed

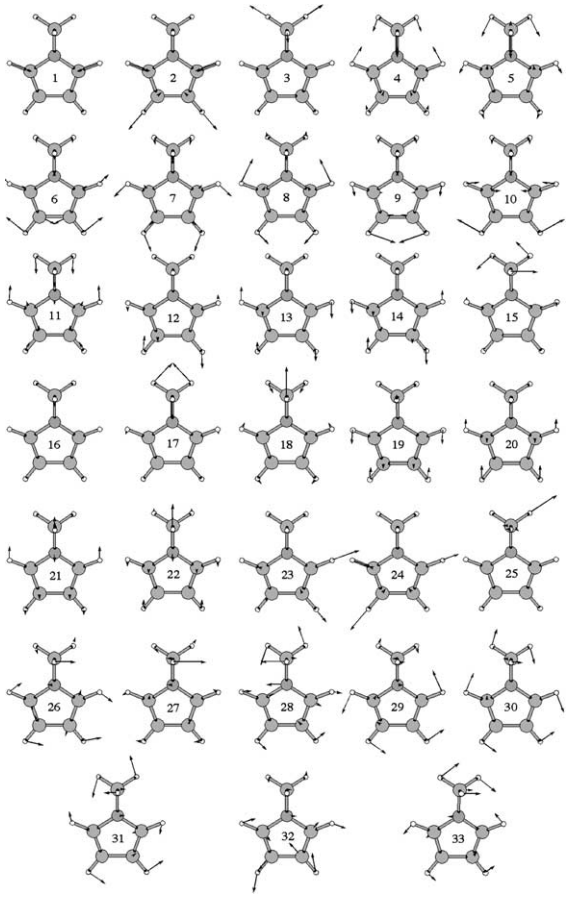

Fig. 4. The ground state normal modes of NMP computed at the B3LYP level using 6-311G** basis set. The molecular plane is tilted 30° out of plane towards the viewer to facilitate viewing the out-of-plane modes (modes 12–15 and 16–22 have a_2 and b_1 symmetry, respectively). Some arrows are not seen because the bonds cover them. The missing arrows are: H9 → C4 and H8 → C3 in ν_1; H12 → C6 and H11 → C6 in ν_{16}; H10 → C5 and H9 → C4 in ν_{23}; H8 → C3 in ν_{24}.

normal modes are always higher than the observed ones. Among the four sets of frequencies, the B3LYP/6-311G** set has the best overall agreement with the experimental data. Fig. 4 depicts all the normal modes. A more descriptive picture of the five active out-of-plane b_1 modes is given in Fig. 5.

5.2. Methyl internal rotation

The torsional potential was calculated using the relaxed scan method available in the Gaussian suite of programs. The torsional angle was scanned in the steps of 2° while optimizing all other parameters for each angle. Table 5 gives the total

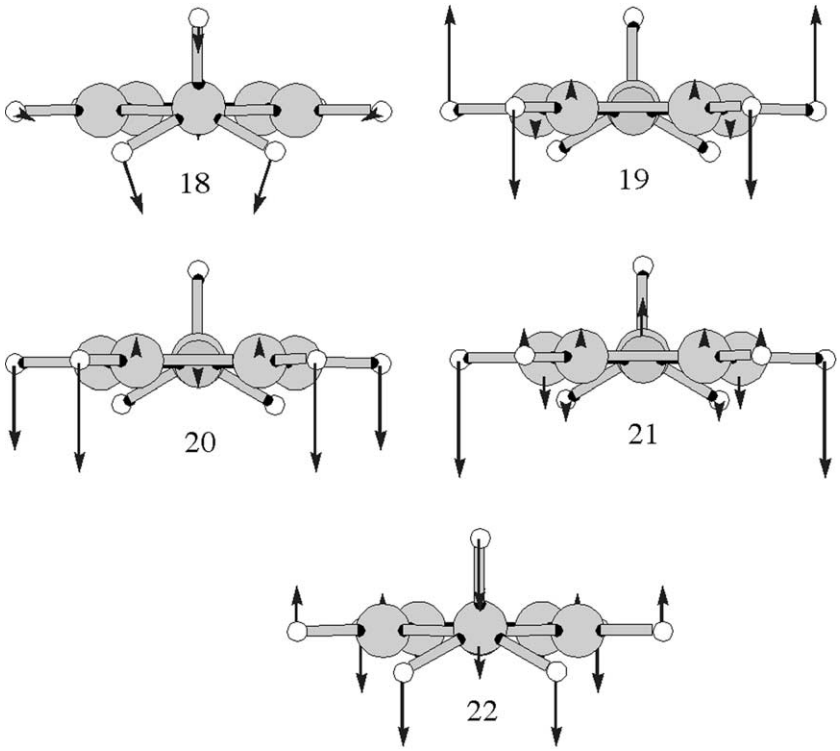

Fig. 5. Redraw of the 18–22 out-of-plane normal modes (b_1) of NMP. For modes 18 and 22 we are looking down from the methyl end of the molecule. For modes 19, 20 and 21 we are looking down from the other end.

Table 5
Methyl torsional barrier computed using various basis sets

	B3LYP/D95++	MP2/D95++	MP2/6-311G**
El. energy (eq)	−249.4472867	−248.3179078	−248.7832213
El. energy (tr. state)	−249.4472056	−248.3176986	−248.7829688
El. barrier (cm^{-1})	17.8	45.9	55.4
ZPE (eq) (cm^{-1})	24318.7	23576.1	24218.1
ZPE (tr. state) (cm^{-1})	24324.9	23534.2	24215.6
Vib. barrier (cm^{-1})	6.2	−41.9	−2.5
Total barrier (cm^{-1})	24.0	4.0	52.9

Electronic energy (first two rows) is expressed in hartrees all other energies are in wavenumbers.

electronic energies and the zero-point vibrational energy (ZPE) calculated using both the basis set. The ZPE was derived by taking half the sum of all vibrational frequencies except the torsion of the methyl group. The torsional mode was considered to be adiabatic while computing the differences in the ZPE between the equilibrium state and the transition state. For the double zeta basis set the numbers obtained using the DFT method are also given. It can be seen that the DFT method gives a very poor estimate of the electronic barrier and further it predicts higher ZPE for the transition state. The MP2 level calculation with the DZ++ basis set gives a good estimate of the electronic barrier. However, the difference ΔZPE is so large that it almost cancels the electronic barrier giving the total barrier of only 4.0 cm^{-1}, which is in poor agreement with the experimentally determined barrier for the internal rotation [1,2,16]. At the MP2 level, using the 6-311G** basis set, the electronic barrier was computed as 55.4 cm^{-1} with a transition state at the eclipsed conformation. The ΔZPE was computed to be -2.5 cm^{-1} giving an overall barrier of 52.9 cm^{-1}. This is in reasonably good agreement with the experimental barrier for the internal rotation of 45 cm^{-1}. The poor estimate of the electronic barrier at the B3LYP level indicates that is does not recover the correlation energy sufficiently. The large difference in the ZPE at the MP2 level using the double zeta basis set was attributed to the large reduction in the normal mode frequency of one of the out-of-plane ring deformation mode, ν_{21}, of b_1 symmetry under the C_{2v} point group. In a theoretical study of the methyl rotational barrier in toluene [17], Hameka and Jensen have found that inclusion of the ZPE in the calculations is necessary for obtaining satisfactory results.

6. Conclusions

The $(A_2)S_1 \leftarrow (A_1)S_0$ transition (Rydberg 3s) of jet-cooled NMP has been investigated by fluorescence excitation and dispersed single level fluorescence spectroscopy. The transition is electric dipole forbidden but vibronically induced. The point symmetry C_{2v} is used. The study revealed that the out-of-plane b_1 vibrations are the active (inducing) modes. The b_1 modes derive their strength through vibronic coupling between the $(A_2)S_1$ excited and the close lying B_2 $\pi\pi^*$ valence state. In-plane vibrations of b_2 symmetry are also active but weak; in this case the intensity is "borrowed" from the B_1 state which is the $3p_y$ Rydberg state. The dispersed fluorescence spectra after exciting the CH_3 internal rotational levels, showed that there is no relaxation to the S_1 zero-point level. For the assignment of the DF spectra, ab-initio calculations have been carried out at the DFT and MP2 levels of theory and the description of the 33 modes of NMP is given. Also, the methyl internal rotation potential barrier was calculated and compared to the -45 cm^{-1} experimental value (S_0 state). The present work confirms a previously given conclusion [1] that the conformation of NMP is staggered in the S_0 state and eclipsed in the 3s (A_2) state.

Acknowledgements

We express our thank to Dr. Asuka Fujii (Tohoku University, Japan) for the provided help in making Figs. 4 and 5. JGP thanks Dr. Nobuaki Kanamaru (Nagoya University, Japan) for stimulating discussions during the course of this work.

References

[1] J.G. Philis, Chem. Phys. Lett. 353 (2002) 84.
[2] J.G. Philis, J. Mol. Struct. 651 (2003) 567.
[3] A.L. Sobolewski, W. Domcke, Chem. Phys. Lett. 321 (2000) 479.
[4] G. Milazzo, Gazz. Chim. Ital. 74 (1944) 152.
[5] R. MacDiarmid, X. Xing, J. Chem. Phys. 105 (1996) 867.
[6] C.D. Cooper, A.D. Williamson, J.C. Miller, R.N. Compton, J. Chem. Phys. 73 (1980) 1527.
[7] D.W. Scott, J. Mol. Spectrosc. 37 (1971) 77.
[8] T.J. Dines, L.D. MacGregor, C.H. Rochester, J. Col. Interface Sci. 245 (2002) 221.
[9] S. Huber, T.-K. Ha, A. Bauder, J. Mol. Struct. 413–414 (1997) 93.
[10] H. Takeuchi, K. Inoue, J. Enmi, T. Hamada, T. Shibuya, S. Konaka, J. Mol. Struct. 567–568 (2001) 107.
[11] R.S. Mulliken, J. Chem. Phys. 23 (1955) 1997.
[12] F.M. Garforth, C.K. Ingold, J. Chem. Soc. (1948) 417.
[13] G.H. Atkinson, C.S. Parmenter, J. Mol. Spectrosc. 73 (1978) 52.

[14] M.J. Frisch et al., GAUSSIAN 98, Revision A.7, Gaussian, Pittsburgh, PA, 1998.
[15] S. Huber, J. Makarewicz, A. Bauder, Mol. Phys. 95 (1998) 1021.
[16] W. Arnold, H. Dreizler, H.D. Rudolph, Z. Naturforsch. 23a (1968) 301.
[17] H.F. Hameka, J.O. Jensen, J. Mol. Struct. (Theochem) 362 (1996) 325.